

Chemical structure of grain-boundary layer in $SrTiO_3$ and its segregation-induced transition: A continuum interface approach

Hui Gu(顾辉)

Citation: Chin. Phys. B . 2018, 27(6): 060503. **doi:** 10.1088/1674-1056/27/6/060503

Journal homepage: http://cpb.iphy.ac.cn; http://iopscience.iop.org/cpb

What follows is a list of articles you may be interested in

Aberration-corrected scanning transmission electron microscopy for complex transition metal oxides

Qing-Hua Zhang(张庆华), Dong-Dong Xiao(肖东东), Lin Gu(谷林)

Chin. Phys. B . 2016, 25(6): 066803. **doi:** 10.1088/1674-1056/25/6/066803

Computational studies on the interactions of nanomaterials with proteins and their impacts

An De-Yi, Su Ji-Guo, Li Chun-Hua, Li Jing-Yuan

Chin. Phys. B . 2015, 24(12): 120504. **doi:** 10.1088/1674-1056/24/12/120504

Study on the defect-related emissions in the light self-ion-implanted Si films by a silicon-on-insulator structure

Wang Chong, Yang Yu, Yang Rui-Dong, Li Liang, Xiong Fei, Bao Ji-Ming

Chin. Phys. B . 2011, 20(2): 026802. **doi:** 10.1088/1674-1056/20/2/026802

TOPICAL REVIEW — Electron microscopy method for the emergent materials and life sciences

Chemical structure of grain-boundary layer in $SrTiO_3$ and its segregation-induced transition: A continuum interface approach*

Hui Gu(顾辉)†

School of Materials Science & Engineering, Materials Genome Institute, Shanghai University, Shanghai 200444, *China*

(Received 8 April 2018; revised manuscript received 14 May 2018; published online 30 May 2018)

Grain-boundary (GB) structures are commonly imaged as discrete atomic columns, yet the chemical modifications are gradual and extend into the adjacent lattices, notably the space charge, hence the two-dimensional defects may also be treated as continuum changes to extended interfacial structure. This review presents a spatially-resolved analysis by electron energy-loss spectroscopy of the GB chemical structures in a series of $SrTiO_3$ bicrystals and a ceramic, using analytical electron microscopy of the pre-C_s-correction era. It has identified and separated a transient layer at the model Σ5 grain-boundaries (GBs) with characteristic chemical bonding, extending the continuum interfacial approach to redefine the GB chemical structure. This GB layer has evolved under segregation of iron dopant, starting from subtle changes in local bonds until a clear transition into a distinctive GB chemistry with substantially increased titanium concentration confined within the GB layer in 3-unit cells, heavily strained, and with less strontium. Similar segregated GB layer turns into a titania-based amorphous film in $SrTiO_3$ ceramic, hence reaching a more stable chemical structure in equilibrium with the intergranular Ti_2O_3 glass also. Space charge was not found by acceptor doping in both the strained Σ5 and amorphous GBs in $SrTiO_3$ owing to the native transient nature of the GB layer that facilitates the transitions induced by Fe segregation into novel chemical structures subject to local and global equilibria. These GB transitions may add a new dimension into the structure–property relationship of the electronic materials.

Keywords: space charge layer, strontium titanate bicrystal, spatially-resolved electron energy-loss spectroscopy, interfacial transition

PACS: 05.70.Np, 68.35.Dv, 68.37.Ma, 81.70.Jb **DOI:** 10.1088/1674-1056/27/6/060503

1. Background on grain-boundary chemistry and space charge

Grain-boundaries (GBs) in $SrTiO_3$ often serve as a model system for interface studies owing to its cubic structure at ambient conditions that minimizes the anisotropic effect on interfacial planes, while the mixed cations enable more opportunities and wide ranges to control or tune the electric and dielectric properties at the interface. High-resolution transmission electron microscopy (TEM) analysis, which traces as well as reduces the quasi-two-dimensional imperfection down to its structural origin,[1–3] treats interfacial structures as discrete atomic columns. In this era of aberration-corrected TEM using a scanning probe (STEM), the analysis of interfacial structures reaches unprecedented lateral resolution, not only in atomic arrangements but also in chemical identity down to each column.[4] However, the GBs as two-dimensional (2D) imperfections are still the singular defects under the thermodynamic landscape, which induce chemical variations especially by segregation of impurities or dopants, owing to their lower chemical potentials than the matrix. In other words, there is a chemical structure of a finite scale around such internal interfaces that is distinctive to the interrupted lattice above the atomistic scale.

Indeed, impurity segregation was found to turn the GB structures into amorphous layers with equilibrium width of ~ 1 nm in certain ceramic compounds.[5,6] A GB "complexions" scheme was later proposed to treat a wide range of GB structures as interfacial "phases" to expand the segregation picture from sublayer to multilayer adsorption, thus rationalizing the amorphous GB as originated from interfacial transition to drive the accelerated grain growth.[7,8] In parallel, a spatially-resolved electron energy-loss spectroscopy (EELS) analysis had identified a specific oxynitride structure for amorphous GB layers in terms of bonding, composition, and width in nitride ceramics.[9,10] Such chemically stable amorphous structure renders the extended GB layer with predictable electro-chemical affinity to serve as native host to segregated cations. In comparison, the amorphous GBs as silica-based layers in carbide and oxide ceramics largely exhibited a transient nature, which could either promote adjacent minor phase or induce anisotropic grain growth.[11–13]

For $SrTiO_3$ as the ternary compound, chemical structures of the model quasi-2D GB and general GB have both been studied extensively, especially the effect and distribution of segregated accepter or doner but under rather different approaches and resolutions. The model GB was focused mainly into core-structure at subatomic level, while the latter

*Project supported by the National Natural Science Foundation of China (Grant No. 51532006), the Fund from Shanghai Municipal Science and Technology Commission (Grant No. 16DZ2260600), the 111 Project of the Ministry of Education, and the Fund from the National Bureau of Foreign Experts (Project No. D16002).

†Corresponding author. E-mail: gujiaoshou@shu.edu.cn

© 2018 Chinese Physical Society and IOP Publishing Ltd

is more into the segregation behavior at a nanometer scale. They both merge to the key issue of charge transfer or redistribution; one performs in a bottom-up approach to build up the electronic map while the other starts top-down to follow the thermo-chemical origin. The concept of space charge has emerged as an outcome of redistribution of defects to account for charge balance at and near such interfaces, which creates inherent non-stoichiometry either as source or sink to accommodate the excessive defects as demonstrated in Fig. 1 (readapted from Refs. [14] and [15]). The chemical structure of the GB extends from the core-structure to the accompanying space charge zones, this bridges and combines the two approaches across multiscales. Furthermore, such chemical equilibration between the GB core and space charge zone can be tuned or altered by selective segregation of the acceptor or donor.[16–18] Therefore, chemical analysis at subnanometer scale is necessary to probe into the extended GB structure to fully understand functional effects of the GB in $SrTiO_3$ materials.

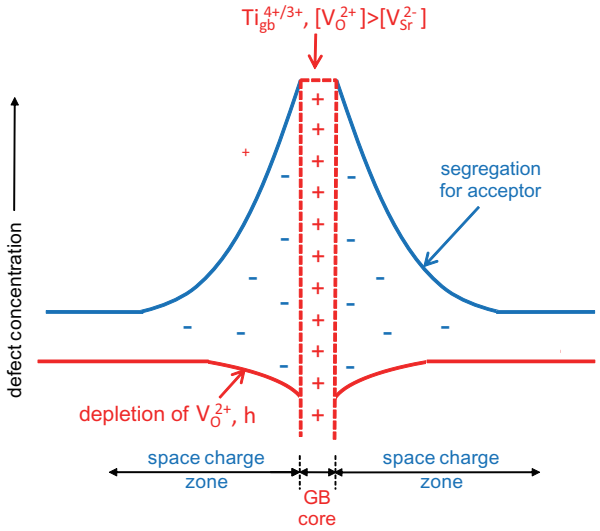


Fig. 1. (color online) Schematic diagram of space charge model for GB non-stoichiometry to accommodate intrinsic defects in $SrTiO_3$; adapted from Refs. [14] and [15]. This extended configuration of GB chemistry receives acceptor dopant by their segregation to the space charge zones.

In 1990s, analytical electron microscopy (AEM) had developed into a matured methodology suitable for probing extended chemical structure of the GB, especially by spatially-resolved EELS. This spectroscopy is sensitive to both the elemental and electronic distribution at a subnanometer scale, especially when such quantitative inquisition could reveal inherent correlation between the chemistry and spatial scale, although it remains largely a continuum approach.[19] Nevertheless, it would be handy to associate with the atomistic studies via quantification of a collection of chemical parameters for the probed interface,[20] hence is still useful in this age of aberration-corrected STEM. In this review of AEM analysis, an extended abstract for a conference[21] and an unpublished internal report from the pre-C_s-correction age have been combined. I present a comparative study of chemical structures of model Σ5 GBs and a general GB with amorphous film in $SrTiO_3$, from intrinsic interfacial layer to associated transition induced by acceptor segregation, ready for further verification by dielectric properties of individual GBs or calculated using integrated modeling.

2. Chemical structure of undoped Σ5 GB layer

Dopant and defect segregation to GB is an inherent chemical property of polycrystalline materials associated with intrinsic and extrinsic chemical defects. This constitutes a thermodynamic variable that could be measured as excess of a chemical constituent segregated to GB above its concentration in the lattice, even by an inquisition probe in the order of 10 nm. The "spatial-difference" technique was developed initially to reveal the weak segregation that often buried under huge background, especially in EELS analysis. This technique improved the detection limit below one atom per nm^2 area of an interface or GB to enable direct correlation of the excess with local atomic structure and chemical bonding.[22] To probe into the native amorphous layer at ceramic GBs, this technique was further developed into a quantitative methodology for GB chemistry, starting by identifying characteristic EELS near-edge structure (ELNES) signals specific to GB layers.[19] By systematic spectral processing via "ELNES separation", full spectrum exclusively for a GB layer could also emerge; hence, its chemical composition and associated width were concurrently obtained, even when the effective probe size was significantly larger than GB layer.[10] However, such an analysis leads to loss of detailed information inside the GB layer, hence it is ideally applicable for the GB layer with a distinctive and uniform structure such as an amorphous film. On the other hand, such interactively identified GB layer may or may not be one useful for the "complexions" scheme that focuses onto structural changes induced by layered transition of chemical adsorbates segregated to GB core.[8] Hence, it minimizes or even trivializes the inherent properties from the adjacent lattices especially the effect from their misorientation relationship, which may be true only in the case of amorphous GB layer.

"ELNES separation" methodology applied to the GBs in $SrTiO_3$ is effectively a cut-off method for continuum tails to identify a GB layer with significant structural modification manifested in characteristic bonding including, but not limited to, the GB core. Such distinctive bonding might change gradually within this GB layer of finite width, no matter whether it is associated with the segregated dopant that might reconstruct the core structure, or with the intrinsic defects that may not alter the structural coordination. Extrinsic defects induced by dopant segregation could combine both into a further extended GB layer, especially for acceptor that is expected to segregate to the space charge zone that expands to tens of nanometers outside the GB layer (Fig. 1).[14,18]

Therefore, a series of GBs in $SrTiO_3$ were selected for this spatially-resolved EELS analysis for the comparative study of the GB chemical structures, namely Σ5 GBs from

bicrystals and amorphous GBs in a ceramic material. These bicrystals were created by cutting along the (310) plane of single crystals and reorienting the two pieces into 36.5° symmetric boundaries around the common [001] direction. The bicystals were then reheated under hot-pressing, and were doped with 0 wt%, 0.1 wt%, and 0.5 wt% of Fe_2O_3 respectively before purchasing from commercial source (Wako Busan, Tokyo, Japan); the ceramic $SrTiO_3$ was hot-pressed and doped with 0.8 mol% of Fe_2O_3; more details about materials processing can be found in an earlier publication.[16] The TEM specimens were mechanically sliced and ion-milled until perforation. The experiments were performed in a dedicated STEM of Vacuum Generator (model HB501, Cambridge, UK) at an accelerating voltage of 100 kV, which offered an analytical probe with sufficient beam current of diameter less than 1 nm. A parallel electron spectrometer (model 666, Gatan Co., Pleasanton, California) was used to acquire EELS spectra. This STEM/EELS system provided an energy resolution of 0.7 eV for ELNES investigation at energy dispersions of 0.3 eV/channel–0.5 eV/channel at the photodiode array, while it degraded to 1 eV for compositional measurements at the dispersions of 1.0 eV/channel.[19] When acquiring an EELS spectrum, a low-angle annular dark-field (LAADF) detector was placed to limit EELS collection within an angle of 6.5 mrad. In the meanwhile, this detector could acquire a LAADF image in an angular range of 6.5 mrad–20 mrad along with a high-angle annular dark-field (HAADF) detector image in the high-angle range of 35 mrad–160 mrad, during the "spectrum-image" acquisition mode of EELS spectra by the scanning probe.[19]

2.1. Experimental procedures for two modes of EELS analysis of GB

The methodology of spatially-resolved EELS analysis of GB includes two different modes in experimental setups, followed by systematic spectral processing, as demonstrated with an $SrTiO_3$ bicrystal to reveal the chemical structure of a Σ5 symmetric GB viewed along the common [001] zone-axis [Fig. 2(a)]. The first mode is spectrum-profiling, as shown in Fig. 2(b), which is the one-dimensional (1D) version of the "spectrum-image" to form a series of spectra acquired when the probe is concurrently line-scanning across this GB. Such spectrum profiling may be obtained in two forms, one showing 40 spectra uniformly and laterally distributed over a distance of 10 nm and the other shifting every 0.25 nm to record a spectrum, as shown in Fig. 2(c). Both Ti–$L_{2,3}$ and O–K edges, starting at 456 eV and 532 eV respectively, are clearly visible along with the four-fold splitting in white-lines. The other mode is much simpler in which two spectra are acquired in frame-scans, one on GB and the other off GB from the adjacent lattice, as also shown in Fig. 2(b). Both frames were in an area of 3 nm×4 nm, which covers a minimal amount of the adjacent lattice while enabling the correction of drifting during the acquisition in typically 20 s; the frame width across the GB should include the effective probe size, hence to reach 5 nm, which is useful in quantification.[10]

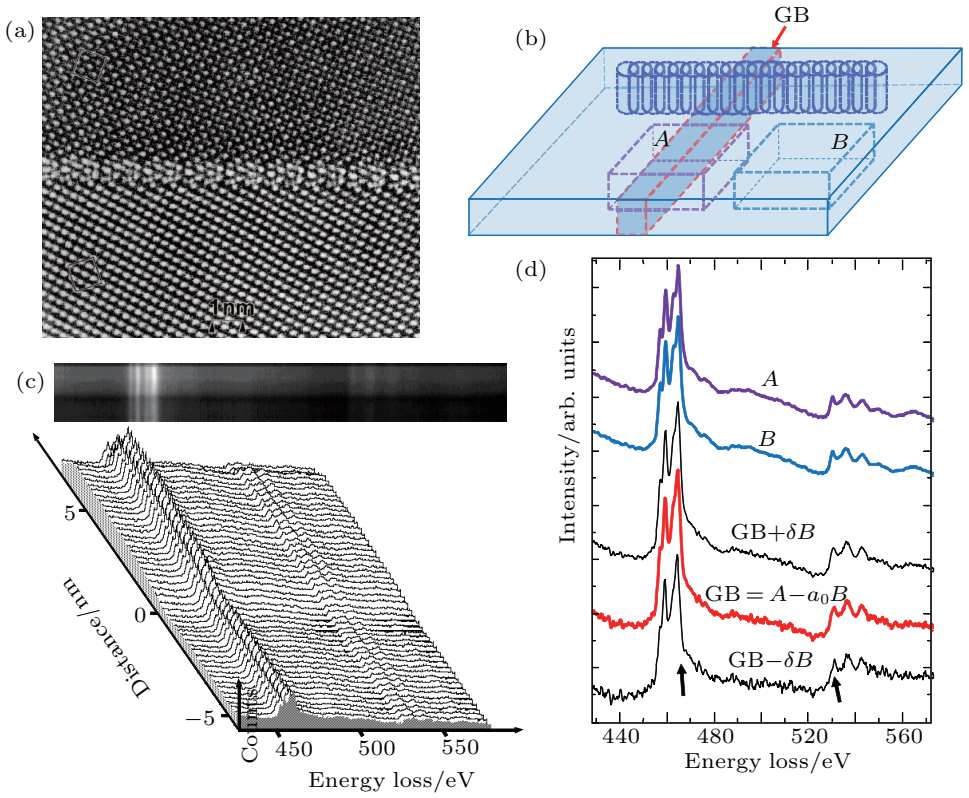


Fig. 2. (color online) Spatially-resolved EELS analysis of Σ5 (310)/[001] GB in $SrTiO_3$ bicrystal: (a) high-resolution TEM image; (b) schematics of the experimental setups for two analytical modes, spectrum-profiling, and ELNES-separation; (c) spectrum-profiling presented in 2D (above) and 3D (below) view; (d) spectral processing by ELNES-separation to retract exclusive spectrum of GB layer (red) from the two spectra *A* (purple) and *B* (blue), measured in scanning frames on and off this GB (more details in the text).

To gain a dedicated spectrum exclusively for the GB layer, off-line spectral processing is necessary for both modes in a similar way as demonstrated for the two-frame mode in Fig. 2(d). The on-GB spectrum A is subtracted from the off-GB spectrum B in increasing amount by small increments (δB) to approach the spectrum specific to the GB layer (labeled GB). When the subtraction is over-due, it appears with unrealistically sharp features in ELNES of either edge (arrows in Fig. 2(d)), owing to the limited possibilities of GB layer by either chemical shift or feature broadening with respect to ELNES pattern of $SrTiO_3$ lattice. The spectrum of GB is then equivalent to the difference of spectrum A and spectrum B in a large fraction (a), or GB $= A - a_0B$, obtained iteratively from this procedure. Similar procedure of spectrum subtraction is applicable to the spectrum-profiling by integrating spectra over certain distances on and off GB. More details can be found in Ref. [10]. From respective intensities in these spectra as well as the frame size or profiling distance, quantification of various chemical parameters is possible according to Ref. [10].

2.2. ELNES and distribution for intrinsic Σ5 GB

This processed ELNES patterns of Ti–$L_{2,3}$ and O–K edges, corresponding to a finite layer of intrinsic Σ5 GB, are shown in Figs. 3(a) and 3(b), respectively together with corresponding ELNES pattern of bulk $SrTiO_3$ acquired from the nearby grain. The GB spectrum reveals no chemical shift at the threshold of Ti–L edge, while the crystal-field splitting of 2.2 eV is shrunk by ~ 0.3 eV for both L_3 and L_2 white-lines as marked by dashed lines between the GB and grain ELNES pattern shown in Fig. 3(a). This splitting originated from the hybridization of Ti-3d and O-2p orbitals in 6-fold coordination, and this mild reduction reflects the distortion of Ti–O_6 configuration around the GB core. For O–K ELNES pattern as shown in Fig. 3(b), no shift of pre-peak indicates the robust Ti–O_6 coordination, but the first main peak shifts by ~ 0.6 eV to the high energy side, which reflects the change in hybridization of O-2p with Sr-4d/5s orbitals.[23] Nevertheless, more elaborate modeling is necessary to reveal detailed structural changes by such variations in ELNES pattern for the intrinsic Σ5 GB.

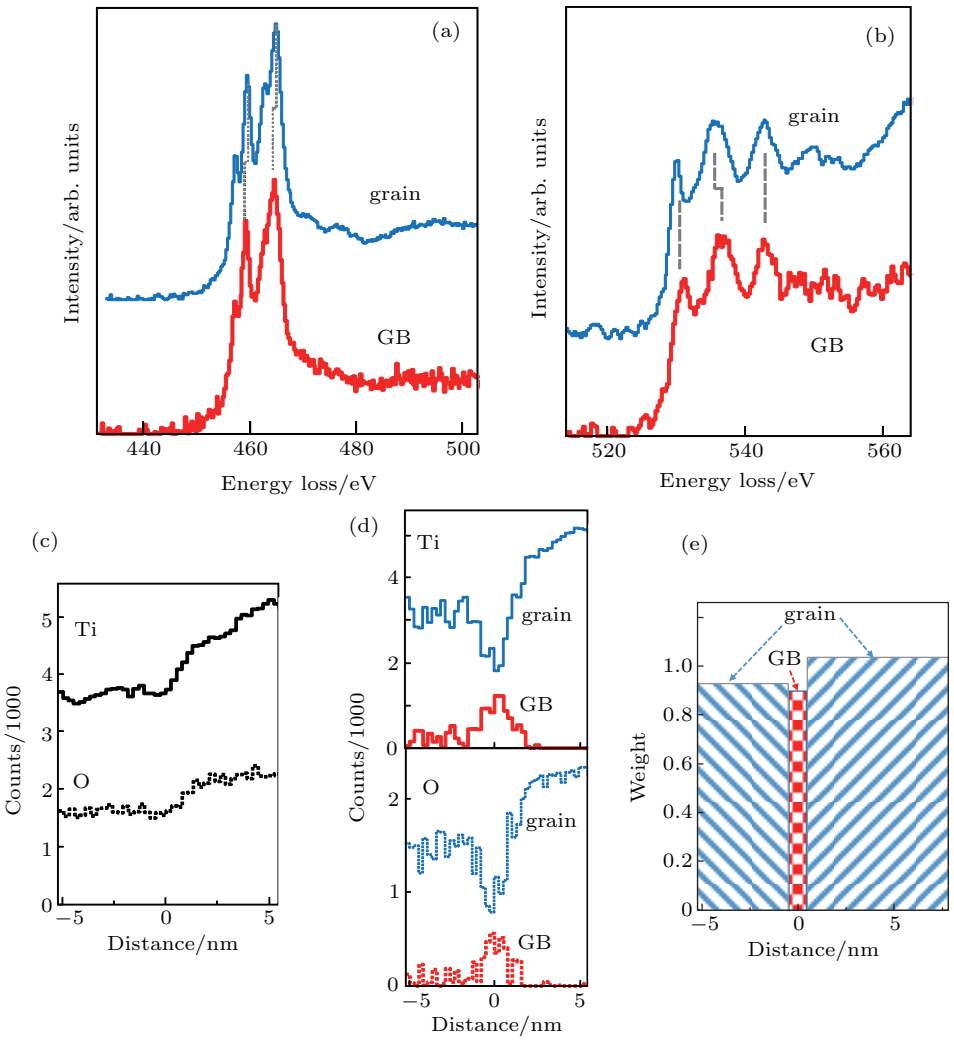


Fig. 3. (color online) ELNES-separation into signals from GB layer (red) and from the lattice grain (blue) for Σ5 (310)/[001] GB in undoped $SrTiO_3$ bicrystal for: (a) Ti–$L_{2,3}$ and (b) O–K edges; (c) elemental and (d) ELNES profiles of Ti–$L_{2,3}$ (above) and O–K (below) signals. Each pair of ELNES profiles could be normalized successively to gain GB concentrations of $\sim 90\%$ of grains and chemical width of 0.8 nm (e); refer to text for more details.

This spatially-resolved EELS methodology can derive further chemical information from this GB layer, which is better presented by the off-line processing for spectrum-profiling as demonstrated in Fig. 2(c). By integrating signals of Ti–$L_{2,3}$ and O–K edges from each spectrum after removal of their backgrounds in a collective processing mode, titanium and oxygen distributions across this undoped Σ5 GB are obtained as shown in Fig. 3(c). These reveal slightly less concentrations for both elements in this undoped GB layer that appears to be ∼ 2-nm wide, although there is a stronger thickness difference between the two grains by ion-milling. By taking summed spectra on either grain from a distance of 2 nm from GB center, subtraction procedure similar to Fig. 2(d) was performed to obtain the spectra specific to GB, like those given in Figs. 3(a) and 3(b). Fitting both ELNES patterns of GB and $SrTiO_3$ grain to all the spectra in this EELS profiling, we obtain two pairs of partial profiles, shown in Fig. 3(d), for Ti–$L_{2,3}$ (upper) and O–K (lower) edges respectively. Signals from this intrinsic Σ5 GB are clearly identified and separated from the adjacent grains, and they are distributed over a width of 1.8 ± 0.2 nm measured at half-maxima of their intensity. The effect of probe expansion through the thickness of the thin TEM specimens is clearly visible: at the position of maximal intensity of GB signals, the grain signals become even higher, indicating that the effective probe had extended well into both grains even when the probe was placed at the middle plane of Σ5 GB.

To derive more information from this GB layer, such severe probe broadening should be modeled for probe shape before deconvolution. Alternatively, this could be removed by a simple deconvolution method that requires no modeling of probe intensity profile,[10] as demonstrated in Fig. 3(e). First, the intensity in the partial profile of grain signal is matched with uniform distribution of both grains by taking their average levels, while maintaining the total intensity unchanged. This creates a gap of no intensity between the two grains to measure the chemical width for this intrinsic Σ5 GB, that is 0.8 ± 0.1 nm or slightly wider than two unit cells of $SrTiO_3$ lattice. Furthermore, by fitting the total intensity of partial profile of the GB signals into this width uniformly, the concentration of corresponding element within this width with respect to its level in the lattice is measured. Since the grain thickness is not the same from both sides of this GB, this results in two GB concentrations differing by 10% and averaging at 90% of their grain levels for both Ti and O. Given that the processing uncertainty for GB ELNES is less than 10%, the relative concentrations are estimated at $90 \pm 10\%$ for both the elements. All the derived chemical parameters of this undoped Σ5 GB are given in Table 1 along with the parameters for other GBs described in the next section.

Table 1. Chemical parameters of GB layers obtained using the spatially-resolved EELS analysis.

Fe_2O_3-dopant	GB type	Width/nm	Relative concentration		Composition			Fe excess/nm^{-2}
			Ti	O	O:Ti	Fe:Ti	Sr:Ti	
No	Σ5	0.8 ± 0.1	0.9 ± 0.1	0.9 ± 0.1	3.0 ± 0.1	0	1	0
0.1 wt%	Σ5	1.3 ± 0.2	1.0 ± 0.2	1.0 ± 0.2	3.0 ± 0.2	< 0.02	1	< 0.5
0.5 wt%	Σ5	1.1 ± 0.1	1.4 ± 0.2	1.2 ± 0.2	2.7 ± 0.1	0.06	0.65	1.5
0.5 wt%*	Σ5	0.4 ± 0.1	1.1 ± 0.1	0.9 ± 0.1	2.4 ± 0.2	?	0.3	?
0.8 mol%	film	1.1 ± 0.2	0.8 ± 0.2	0.6 ± 0.2	2.4 ± 0.2	0.14	0.3	2.3
	TP glass	–	–	–	2.1 ± 0.1	0.55	0	–

3. Effect of acceptor-doping on chemical transition of GB layers

Segregation of Fe to the GB was successfully detected only for high levels of Fe_2O_3 doping, either at 0.5 wt% for bicrystals or 0.8 mol% for ceramics, measured as excess as listed in Table 1. It is worthwhile to notice that the chemical widths of the doped GBs are all in the range of 1.1 nm–1.3 nm as measured by this ELNES-based analysis, or about three unit cells of $SrTiO_3$ lattice across the GB, except for a special case (marked by *). There were two TEM specimens prepared for Σ5 GB with 0.5 wt% of Fe_2O_3 doped into the bicrystal, and Fe segregation was detected only in one specimen; for the other specimen, GB width was measured as merely 0.4 nm, indicating that there exist two rather different chemical structures for this same Σ5 GB.

As shown in Figs. 4(a) and 4(b) respectively for these two cases, concentrations of Ti and O in such two GB layers are also different. In the "good" case with Fe segregation found, significant Ti enrichment is clearly visible at the GB, and it is not the case for "bad" GB layer where Fe was not detected. Similar spectrum-profiling scheme measures Ti excesses at GB as 40% and 10% above the grain level, respectively for the two cases, while O excesses are at 10% and −10% correspondingly; all values are tabulated in Table 1. Furthermore, their ratios within respective GB layers are both clearly lower than the bulk Ti:O level of 3.0, one at 2.7 and the other at 2.4, from which the corresponding Sr:O ratios can be further calculated at 0.65 and 0.3, respectively, by matching to stoichiometry while retaining all Ti^{4+} at the GB. It is possible for small number of Ti^{3+} with Ti^{4+} to co-exist in the GB layer, and this would raise the estimated Sr:O ratio accordingly. On the other hand, deficiency in Sr can be measured, using EDS analysis, as negative excess of segregation to the GB,[24] which was unfortunately not carried out in the current experiment that was performed much earlier. Nevertheless, by ELNES analysis, the level and character of Sr in these GB layers could still be compared between the "good" and "bad" cases for Fe segregation.

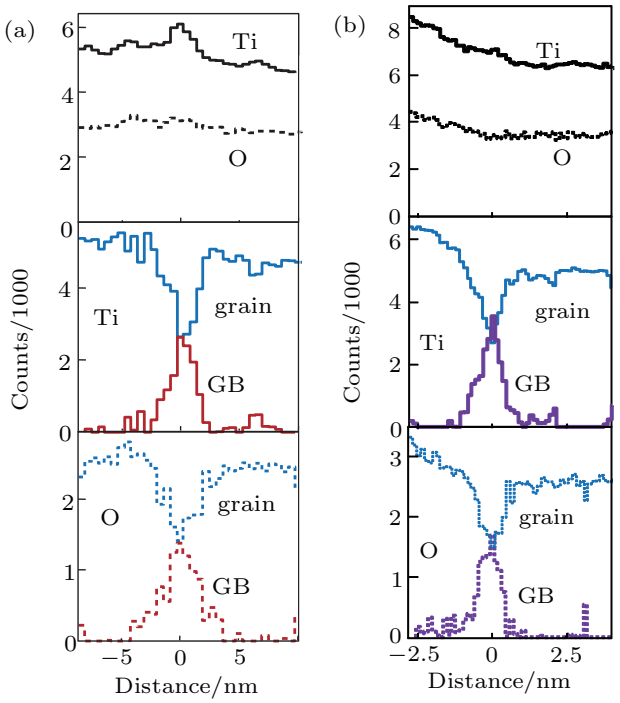


Fig. 4. (color online) (a) and (b) EELS profiling for two Σ5 (310)/[001] GBs in an $SrTiO_3$ bicrystal doped with 0.5 wt% of Fe_2O_3: elemental (top) and ELNES profiles (middle, bottom) of Ti–$L_{2,3}$ and O–K edges, respectively. The second GB (b) may originate from partial fracture along its plane; refer to text for more details.

3.1. Strained Σ5 GB layer by segregation of iron

Indeed, O–K ELNES patterns from these Σ5 GB layers exhibit trends of chemical change owing to increase in percentage of Fe_2O_3 dopant, as shown in Fig. 5. Besides the pre-peak from Ti-3d/O-2p hybridization orbitals, the two main peaks correspond to the overlapping of O-2p with Sr-4d/5s and Ti-4p/4s orbitals, respectively.[23] The first main peak shifts systematically to higher energy, indicating that Sr-O coordination in Σ5 GB was modified increasingly by Fe segregation. For the chemical structures of both the undoped and 0.1 wt% doped Σ5 GB layers are moderately different from $SrTiO_3$ lattice, hence there is no significant change in bonding or composition. In contrast, 0.5 wt% of Fe_2O_3 doping not only changes the Sr–O bonding for Σ5 GB significantly, but also causes an increase in Ti concentration (Fig. 4(a)) leading to a relative decrease in Sr concentration. The linkages between Ti–O_6 coordination should be in a more compact arrangement, most likely to change from corner-sharing to edge-sharing for some, which leaves less space for Sr cations and is also similar to rutile TiO_2 structure. In other words, a transition of chemical structure induced by Fe segregation occurs in Σ5 GB layer turning it into a heavily distorted GB structure with mixed linkages between $SrTiO_3$ and TiO_2 structures. Unfortunately, the energy resolution in the experiment was lowered owing to the setting of the energy dispersion to 0.5 eV/channel for detection of Fe segregation at this Σ5 GB; this led to insufficient details in ELNES to reveal further information for such a GB transition.

On the other hand, another chemical structure, which is even more similar to rutile structure as revealed in Fig. 5 (marked by symbol ∗) was found for "bad" Σ5 GB after 0.5 wt% Fe_2O_3 doping. Indeed, it is hard to find the first main peak representative for Sr-O bonding in its O–K ELNES pattern, while the Ti:O ratio decreases from 2.7 to 2.4, bringing the structure further close to that of TiO_2 (see Table 1). This second chemical structure not only has absence of enrichment of Ti, but its width has also shrunk to 0.4 nm, which is merely one unit cell wide across this "bad" GB.

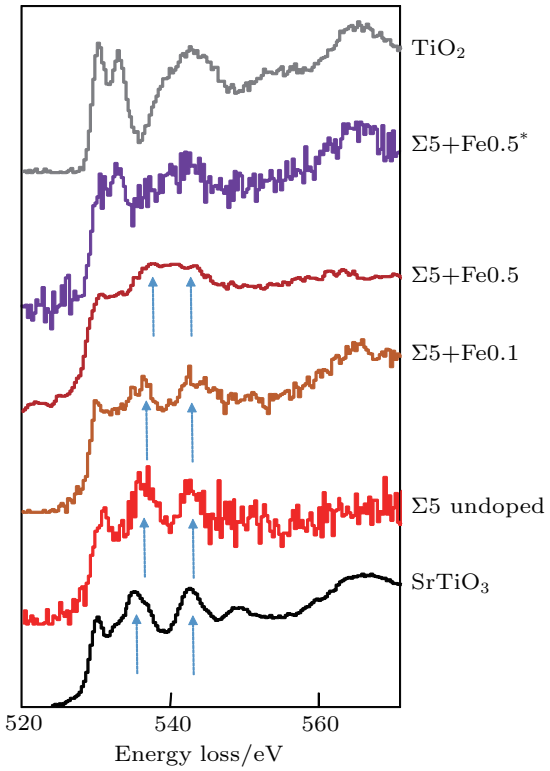


Fig. 5. (color online) ELNES of O–K edges from Σ5 (310)/[001] GBs in $SrTiO_3$ bicrystals, doped with different amounts of Fe_2O_3 dopant. Two GBs from the bicrystal with 0.5 wt% of dopant are present, and the one corresponding to Fig. 4(b) is marked with symbol ∗, together with ELNES of $SrTiO_3$ and rutile TiO_2.

These two chemical structures for Fe-segregated Σ5 GB might be further correlated with each other in a further transition. The heavily distorted bonding and clearly higher density of Ti–O_6 coordination stores tremendous amount of strain into this GB layer under hot-pressing, as witnessed by 40% and 20% increase for Ti and O, respectively, within a width of 1.1 nm. The first chemical structure of strained GB has a mixture of Ti–O_6 linkages in both the corner-sharing and edge-sharing configurations, ready to release the strain from the confined layer especially during the thinning process for preparing TEM specimens. The second chemical structure of this "bad" GB is probably a result of such a release of GB strain, not only due to lack of concentration excesses, but also because of much thinner GB layer owing to the possible demixing of corner-sharing and edge-sharing Ti–O_6 configurations. This leaves the latter to fill one third of the spacing

between two unaltered grains. Indeed, along this GB and hundreds of nanometers far from the area for the "bad" GB structure, visible cracks were observed. In other words, the strained GB structure may be half a transition to create mixed Ti–O_6 configurations into the strained, extended GB layer confined into no more than 3 unit-cells.

3.2. Chemical structure of amorphous GB film

In light of the revelation of chemical transition for Σ5 GB induced by Fe segregation, chemical structure of the general GB in $SrTiO_3$ ceramic was also analyzed using this spatially-resolved EELS analysis. GB structures in ceramics are usually in unknown misorientations between two grains, which form either in an amorphous film of ∼ 1 nm thickness, or without any amorphous or crystalline film. One such GB film is observed in both LAADF and HAADF images as shown in Fig. 6 and is also confirmed by associated chemical changes. ELNES of both Ti–$L_{2,3}$ and O–K edges specific to this film were obtained in same spectra via ELNES separation process, as given in Fig. 6(b) along with the spectra of $SrTiO_3$ grain and TiO_2 for reference. Double arrows reveal the shrinkage of crystal-field splitting from 2.2 eV in both lattices to 1.4 eV in the GB film, for Ti–L_3/L_2 lines as well as for O–K pre-peak, which reflect the change in hybridization between Ti-3d and O-2p orbitals. This narrowing of the crystal-field splitting may result from reduction of the titanium coordination and/or the valence. In other words, the amorphous network is possibly constructed by a combination of Ti–O_6/Ti–O_4 coordination, which might be more flexible than the mixed linkage of corner-/edge-sharing Ti–O_6 coordination. It is interesting to note that O–K ELNES of the GB film also deviates significantly from both $SrTiO_3$ and TiO_2, with the first main peak almost flattened to indicate strong modification of overlapping electronic density between Sr-4d/5s and O-2p orbitals, especially the reduction in population of Sr–O bonding. All these indicate that the chemical structure of the amorphous GB film constitutes a TiO_2-based random network owing to a combination of Ti–O_{6-x} coordination and linkage.

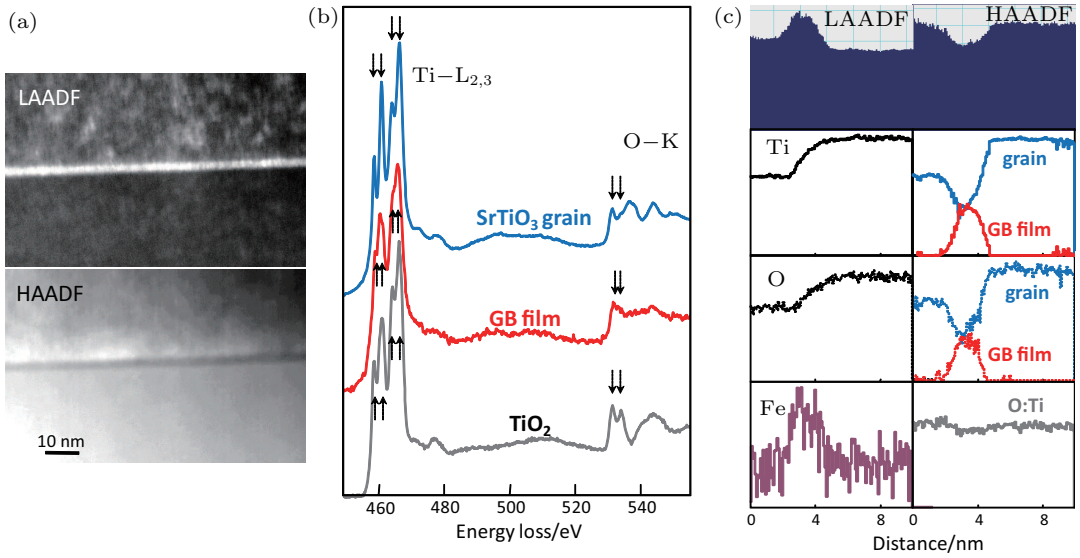


Fig. 6. (color online) Spatially-resolved EELS analysis of amorphous GB film in an $SrTiO_3$ ceramic: (a) STEM images; (b) ELNES separated spectrum of GB film (red) with both Ti–$L_{2,3}$ and O–K edges, together with those from grain (blue) and rutile reference (gray); (c) EELS profiling to generate chemical profiles from STEM intensities (LAADF/HAADF), elemental (Ti, O, Fe), ELNES signals for grain (blue) and film (red) of both the edges, and O:Ti ratio (gray) across this GB.

EELS profiling across this amorphous film reveals more characteristics of its chemical structure, as demonstrated in Fig. 6(c) and also summarized in Table 1. The segregation of Fe dopant to this GB was clearly visible, revealing a rather uniform distribution. In fact, the grain on left side of this GB film was aligned much nearer to a zone-axis than the grain on right side, as indicated by their intensity variation shown in LAADF profile; this makes the opposite variations for both elemental profiles of Ti and O, hence their intensities across GB film were buried and compromised. Nevertheless, by applying ELNES separation method it creates two partial profiles for each edge: both partial profiles of GB ELNES reveal very similar distributions as compared to that of Fe segregation, while both partial profiles of $SrTiO_3$ ELNES demonstrate the same effect of left grain closer to the zone-axis. On the other hand, such an effect could have been cancelled owing to the ratio between Ti and O; a slight decrease in oxygen in the film is visible in this O:Ti profile, which measures as 2.4 down from 3.0 in the grains. By the associated quantification, the chemical width of the GB film measures as 1.1 nm and the relative concentrations of Ti and O in this film were 80% and 60% of their bulk levels, respectively, while Fe concentration was also measurable as 14% of Ti concentration. Further estimation according to stoichiometry in the film can put Sr

concentration to merely 30% of its level in $SrTiO_3$. This confirms a chemical composition of this GB film as TiO_2-based, or $Ti_{0.83}Sr_{0.25}Fe_{0.1}O_2$, thus emerging as a stable and uniform chemical structure for the amorphous GB film.

3.3. Transitions of GB chemical structure by Fe segregation

The detection of Fe dopant segregated within a layer of the GB, at both coherent Σ5 type and general amorphous film, signifies that the space charge layer initiated by the acceptor segregation does not exist in $SrTiO_3$, hence there is no oxygen deficiency in expected configuration at GB core to be balanced by the space charge. Instead, the GB core structure expands by modification of Ti–O_6 linkage network to alter the native chemical structure of 2–3 unit cells into extended GB layer, which concurrently aids taking in more Fe dopant while leaving out some Sr ions due to reduced spaces between the edge-sharing Ti–O_6 coordination mixed with corner-sharing configurations. This situation was compared with full spectra of different chemical structures including Ti–$L_{2,3}$, O–K, and Fe–$L_{2,3}$ edges, as presented in Fig. 7. The spectra of perovskite $SrTiO_3$ and rutile TiO_2 are also included to represent the end members with pure corner-sharing or edge-sharing configurations for Ti–O_6 linkage. Even under such relatively low energy resolution, the hybridized orbitals Ti-3d/O2p, hence Ti-O_6 coordination, were retained through the transition of chemical structure in the GB layer, as is visible from the crystal-field splitting in Ti–L_3/L_2 lines and O–K pre-peaks in all cases. In parallel, evolution of Sr-O bonding environment manifested in O–K ELNES as shift and reduction of the leading peak in ELNES of $SrTiO_3$ into two stages. First, this peak shifted towards high energy to merge into a plateau together with the second peak, corresponding to a first or half transition into the strained GB structure with mixed linkages of Ti–O_6 confined by the Σ5 correlation. Second, this peak flattened to turn the coherent configuration into the random network of amorphous film for general GB, hence reaching an unstrained chemical structure by full transition. The latter is also promoted by the chemical equilibration of titania-based film with titania glass formed at connecting intergranular triple-pockets (TP), as witnessed by their similar ELNES patterns in contrast to rutile structure of ordered edge-sharing Ti–O_6 network.

In the meanwhile, Fe segregation witnesses the transitions by following their randomness in Ti–O_{6x} network as measured in Fe:Ti ratio, which increases more than twice from the mixed linkage in the constrained Σ5 GB to the mixture of octahedral and tetrahedral coordination in the confined amorphous film, and a further four times in the unconfined glass pocket. This behavior for Fe dopant indicates a mode change from segregation to solution in the random network of Ti–O_6/Ti–O_4. This is indeed the favorable chemical configuration to accommodate iron dopant since Fe^{3+} ions act as network-builders and modifiers to replace both Ti^{4+}/Ti^{3+} and much bigger Sr^{2+} ions, especially for the latter in the film, as such randomness tends to decrease the number of coordinated oxygen ions by cation. The chemical composition of the glass pocket is $TiFe_{0.55}O_{2.1}$ without including Sr, or $Ti_{1.43}Fe_{0.79}O_3$ based on Ti_2O_3, whereby Ti^{3+} and Fe^{2+} ions dominate this chemical structure to maintain the stoichiometry with only one-sixth of Fe^{3+} ions among all iron solutes. The chemical formula of amorphous film is estimated as $Ti_{0.83}Sr_{0.25}Fe_{0.1}O_2$ based on TiO_2, and it turns to $Ti_{1.25}Sr_{0.95}Fe_{0.18}O_3$ based on Ti_2O_3 with only Fe^{2+}. In other words, Sr:Ti ratio jumps from 0.3 to 0.86, or nearly three times, by reducing both the solvent and solute cations. The ratio should be in between the two values; 20% lower concentration of Ti cation may give a further estimation, which must be obtained by modeling or experimental references. In addition, Sr deficiency in the GB film is measurable as negative excess to GB by EELS or EDS analysis, which may fully address the chemical composition of GB film.[9,24] In Fe-segregated Σ5 GB layer found also with excessive titanium and oxygen, the chemical composition is $TiSr_{0.65}Fe_{0.06}O_{2.7}$ with Ti^{4+} and Fe^{3+} ions, or $TiSr_{0.68}Fe_{0.06}O_{2.7}$ with Fe^{2+} ions. It is impossible to match Sr level with that of Ti or close since this would raise Ti^{3+} ions to 70%. The opposite case of Ti^{4+} dominance should be true because the heavily strained, more compact Ti–O_6 network can take much smaller Fe ions to fill some Sr sites, while leaving some other Sr sites vacant to resettle for stoichiometry.

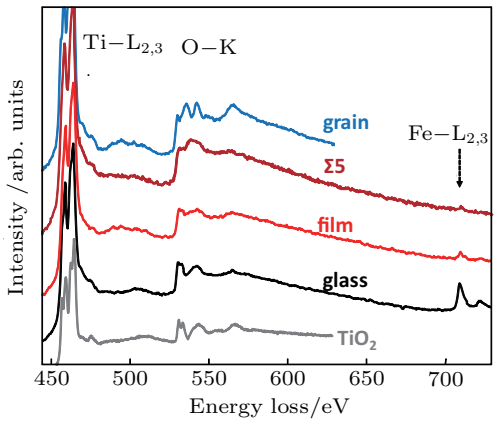


Fig. 7. (color online) EELS spectra of Σ5 GB (dark red), amorphous film (red), and glass triple-pocket (TP, black) to show the effect of Fe segregation onto corresponding chemical structures, as compared with grain (blue) and rutile (grey) reference.

Therefore, Fe segregation modifies the GB structure and expands the core into a layer of 3 unit cells with distinctive chemical structure, effectively inducing a GB transition as schematically depicted in Fig. 8. In fact, the intrinsic Σ5 constitutes subtle difference with $SrTiO_3$ lattice by rearranging the linkage of Ti–O_6 coordination within only the first unit cell at the core plane, while the electric effect extends to the second unit cell via distortion of chemical bonds. Lowered

concentration of Ti and O, perhaps also of Sr, maximizes at the core plane, as depicted in Fig. 8(a), and each sums up to less than 10% over a width of 0.8 nm as defined by ELNES. This intrinsic GB layer is effectively a transient layer with gradual and minimal changes in bonding and electronic structures with little or no apparent shift of lattice column over a range of about 1–2 unit cells, from such as revealed from surface and interface of a VO_2 thin film.[25] Nevertheless, transition of this transient layer to the extrinsic Σ5 GB expands the layer while creating a novel chemical structure with more compact linkage of Ti–O_6 coordination to incorporate segregated Fe while accommodating less Sr, as demonstrated in Fig. 8(b). There is a second or full transition from coherent to incoherent GB structures, or from the strained GB to unstrained film. The latter reverses the higher density of Ti–O_6 coordination to lower than the lattice as described in Fig. 8(c); hence, it relaxes the segregated GB to turn the chemical structure into a more uniform equilibrium film, without further expansion of the GB layer. Indeed, segregated Fe distributes across the entire amorphous film while much lower than in the connected TP, indicating the equilibration between the two amorphous structures.[26] Nevertheless, a segregated cation to GB can only be in equilibration with its solution in the adjacent grains that construct the GB plane, except for cases with a distinctive GB layer of finite width such as an amorphous film. This Fe-segregated Σ5 layer has adjacent lattice taking no solution or a neighboring phase to equilibrate with, while creating the extrinsic chemical structure under the constraint of coherency by the GB plane, which may neither segregate in ceramics nor transform into a similar film.

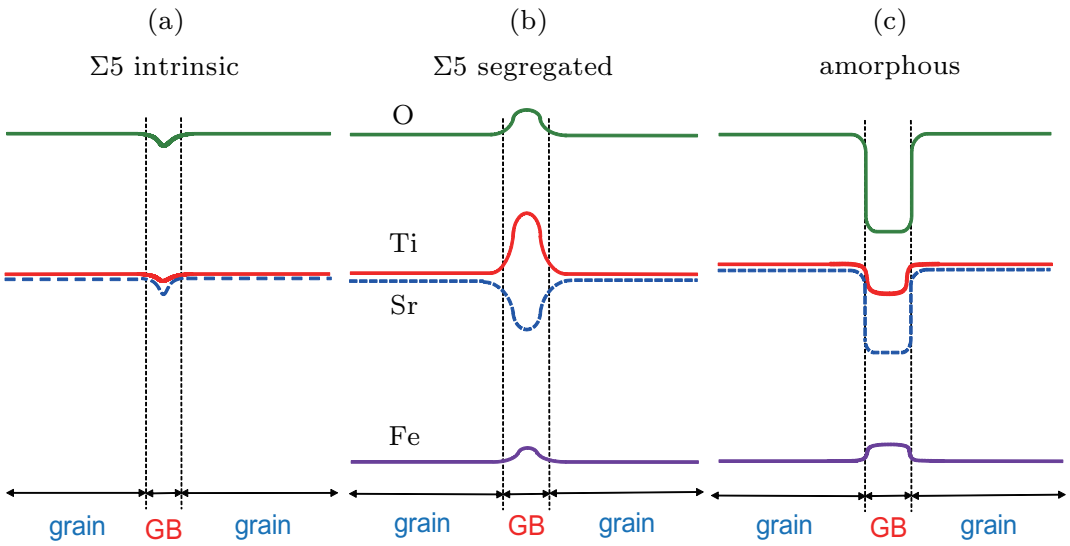


Fig. 8. (color online) Schematics of chemical structures for GB: (a) undoped Σ5, (b) segregated Σ5 and (c) amorphous film to reveal the transitions of GB structure induced by Fe segregation. Dashed vertical lines mark each GB layer of its distinctive chemical structure as resolved by EELS analysis, and none reveals the space charge zone.

Such two transitions (or half-transitions) between these three GBs of $SrTiO_3$ are conceptual and may not realize on the same GB in experiments. This is because there is a scale gap between the local and global equilibria, one reached only a few unit cells out of the GB plane while the other established between correlated thermodynamic identities across the grain scale. The space charge picture (Fig. 1) is the first attempt to combine these two scales, although it was based on the assumption that the grains in the structure are rigid up to the very core of the GB to accommodate chemical defects by the native 2D structural defect, which is true for intrinsic Σ5 GB without doping. A finite layer in a distinct and specific chemical structure can develop at the GB as a new identity to resettle the local equilibrium initiated by the same accepter dopant across, as well as along, the GB, as demonstrated by the first and the second transitions, respectively.

On the other hand, the scheme of the GB complexions was also established to bridge the global and local equilibria by taking the GBs directly as 2D phases to merge into bulk phase diagrams. This may go too far in the opposite direction of the space charge picture, especially for complexion transition to initiate abnormal grain growth hence to dictate development of ceramic microstructures.[8] The GB transition in ceramics must involve TP to reach global equilibrium by connecting the two scales across and along the GB, no matter how the grain was grown in $SrTiO_3$ ceramics as well as in structural ceramics.[9,11,13,24] Facet transition and nanoprecipitation could also occur at the same GB planes, both before and after the grain growth.[27–29] However, such a variety of locally or globally equilibrated chemical structures at the GBs of $SrTiO_3$ can help us to better understand the dielectric properties associated inherently with them, often imprinted into the formation of these chemical structures when interfacial charge could as well play a role.[30]

4. Conclusion and perspectives

This spatially-resolved analysis from the pre-C_s-correction age probes into the electrochemical structure of representative $SrTiO_3$ GBs especially those connected to their immediate neighborhood, although in the absence of precise information down to atomic columns at the GB core. In a continuum approach, this study counters the picture of the space charge induced by the accepter dopant to compensate for non-stoichiometry at the GB core. Instead, distinctive chemical structures, $\sim$ 3-unit cells wide, emerge for both coherent $\Sigma 5$ GB and amorphous GB film. These are effectively created because of two transitions of chemical structures induced by Fe segregation, or two half-transitions, distinguished only by local or global chemical equilibria re-established within this GB layer. Such a quantitative study of chemical distribution to associate it with width makes the resultant chemical information compatible to further detailed studies of electronic structures of the GB structures, especially with theoretical modeling to reveal the chemical interaction at the subatomic scale.

Although this review concentrates only on two cases representing model and general GBs, combining structural and chemical information across various scales should be followed and widened in future TEM studies of the GB structures in $SrTiO_3$ as well as other materials. Even for this work using a low-precision STEM of pre-C_s-correction age, EDS analysis of Sr-deficiency might well complete such analysis of interfacial chemical structures. Theoretical modeling for ELNES patterns will provide further information about structures and physical phenomena within these GB layers, which could be associated with an independent structural analysis under higher resolution than the chemical analysis. In the present age of C_s-corrected TEM, this extended GB picture to include the space charge effect could be further extended to spin ordering effect induced by the interfacial chemical structure, especially in combination with the electron magnetic circular dichroism technique that approaches the nanometer scale.[31] Inclusion of the interfacial magnetic structure may lead to a "hierarchical" interfacial structure with different scales for distributions of segregation, vacancy, charge, and spin order, hence reaching full analysis of interfacial structures. Furthermore, such a variety in chemical structures of the GBs signifies that it is necessary to tune and control dielectric properties by more sophisticated modeling to rationalize systematic experiments in electronic materials, especially in cases across atomic and nanometer scales.[4,18] This comprehensive study of analytical TEM opens a new possibility to establish collective correlation with the electrical behavior of an assembly of GBs via *in situ* and/or *exsitu* experiments, hence expanding the structure-property relationship into a multiscale landscape.

Acknowledgment

The paper is written out of an internal report when the author was a postdoc at then the Max-Planck Institute of Metal Research, as part of a collaboration between the departments of Prof. Manfred Rühle and Prof. Joachim Maier of the Max-Planck Institute of Solid-state Research. Dr. Janick Denk and Prof. Susan Stemmer are acknowledged for their contributions and discussion that lead to this work. Dr. Juan-Juan Xing and Ms. Shu-Ya Zhu for their discussion and help in this manuscript.

References

[1] Kim M, Duscher G, Browning N D, Sohlberg K, Pantelides S T and Pennycook S J 2001 *Phys. Rev. Lett.* **86** 4056
[2] Zhang Z, Sigle W, Philippe F and Rühle M 2003 *Science* **302** 846
[3] Zhang Z, Sigle W, De Souza R A, Kurtz W, Maier J and Rühle M 2005 *Acta Mater.* **53** 5007
[4] Nakagawa N, Hwang H Y and Muller D A 2006 *Nat. Mater.* **5** 204
[5] Clarke D R 1987 *J. Am. Ceram. Soc.* **70** 15
[6] Ziegle A, Idrobo J C, Cinibulk M K, Kicielowski C, Browning N D and Ritchie R O 2004 *Nature* **306** 1768
[7] Tang M, Carter W C and Cannon R M 2006 *Phys. Rev. Lett.* **97** 075502
[8] Dillon S J, Tang M, Carter W C and Harmer M P 2007 *Acta Mater.* **55** 6208
[9] Gu H, Pan X Q, Cannon R M and Rühle M 1998 *J. Am. Ceram. Soc.* **81** 3125
[10] Gu H 1999 *Ultramicrosc.* **76** 173
[11] Gu H, Nagano T, Zhan G D, Mitomo M and Wakai F 2003 *J. Am. Ceram. Soc.* **86** 1753
[12] Huang R, Gu H, Zhang J X and Jiang D L 2005 *Acta Mater.* **53** 2521
[13] Qian P X, Gu H and Aldinger F 2008 *Int. J. Mater. Res.* **99** 240
[14] Chiang Y M and Takagi T 1990 *J. Am. Ceram. Soc.* **73** 3278
[15] Bäurer M, Shih S J, Bishop C, Harmer M P, Cockayne D and Hoffmann M J 2010 *Acta Mater.* **58** 290
[16] Denk J, Claus J and Maier J 1997 *J. Electrochem. Soc.* **144** 3526
[17] Desu S B and Payne D A 1990 *J. Am. Ceram. Soc.* **73** 3391
[18] Waser R 1995 *Solid State Ionics* **75** 89
[19] Gu H, Cěh M, Stemmer S, Müllejans H and Riihle M 1995 *Ultramicrosc.* **59** 215
[20] Gu H and Cěh M 1999 *Ultramicrosc.* **78** 221
[21] Gu H 1996 *Mater. Res. Soc. Symp. Proc.* **458** 115
[22] Bruley J 1992 *Phil. Mag. Lett.* **66** 47
[23] Tanaka I, Nakajima T, Kawai J, Adachi H, Gu H and Rühle M 1997 *Phil. Mag. Lett.* **75** 21
[24] Xing J J, Gu H, Heo Y U, Takeguchi M 2011 *J. Mater. Sci.* **46** 4361
[25] Li X, Gloter A, Gu H, Luo J, Cao X, Jin P and Colliex C 2014 *Scr. Mater.* **78–79** 41
[26] Bobeth M, Clarke D R, Pompe W 2004 *J. Am. Ceram. Soc.* **82** 1537
[27] Xing J J, Gu H, Gloter A, Shen H, Pan X M and Wang P C 2007 *Acta Mater.* **55** 5323
[28] Chi M F, Gu H 2004 *Interf. Sci.* **12** 335
[29] Gu H, Tanaka I, Cannon R M, Pan X Q and Rühle M 2010 *Int. J. Mater. Res.* **101** 66
[30] Clarke D R, Shaw T M, Philipse A P and Horn R G 1993 *J. Am. Ceram. Soc.* **76** 1201
[31] Wang Z Q, Zhong X Y, Yu R, Chen Z Y and Zhu J 2013 *Nat. Commun.* **4** 1395